13th International Brick and
Block Masonry Conference
Amsterdam, July 4-7, 2004

EXPERIMENTAL VERIFICATION OF SETTLEMENT-INDUCED DAMAGE TO MASONRY WALLS

J.J. Loots[1], G.PA.G. van Zijl[2]

Abstract

This paper concerns the simulation of tunnelling-induced settlement damage to solid masonry walls. The design of the test apparatus, the preparation for the test, the test results and the interpretation of the test results are described. The results are compared with simple analytical, as well as finite element predicted responses.

Key Words

Settlement, damage, masonry, finite elements.

1 Introduction

The planned Gautrain is a rapid rail link between the centres of Johannesburg and Pretoria (South Africa). A series of tunnels will be required along this route. Construction of tunnels like these for the planned Gautrain is accompanied by ground movements, which exert extra actions through displacements on the surrounding infrastructure.

In this project a brick wall of length 3 m and height 1 m was built and a laboratory simulation done to gather information on the structural response when vertical ground deformations (settlements) occur. An approximately evenly distributed load was imposed on the wall. The load was variable through displacement-control, so that a comparison could be made between the imposed load and the deflection of the wall. In order to simulate sagging of the foundation, the wall was built on a simply supported steel beam, which was then deflected to act as the vertical ground deformation.

The data gained from this test is analyzed and these results compared to existing methods to analyze the behaviour of brick walls when a settlement trough forms beneath it. Reference is made to the limiting tensile strain (LTS) method (Burland et al. 1974, Boscardin and Cording 1989, Cirillo et al. 2004), while linear elastic, as well as non-linear finite element analyses are performed to simulate the wall response.

[1] J.J. Loots, University of Stellenbosch, South Africa, 13278673@sun.ac.za
[2] G.P.A.G. van Zijl, University of Stellenbosch, South Africa, gvanzijl@sun.ac.za / Delft University of Technology, The Netherlands.

2 The experiment

The information for this report was gathered by means of an experiment done in the structures laboratory of the University of Stellenbosch. All the steps leading to this experiment, the experiment and the results of this experiment are discussed.

The test apparatus was designed to test a solid masonry wall of 3m long, 1m high and 100 mm thick. The concept envisaged was to load the wall to a predetermined load, simulating floor loads, after which the foundation would be deformed to simulate a settlement trough directly under the wall. However, to avoid immediate failure in this scenario upon simulation of the trough, it was decided to superimpose a smaller top load before deforming the foundation. Subsequently, the top load was increased to study the load-deformational response, including wall bridging and damage development according to the damage classification by Boscardin and Cording (1989), Table 1. This table provides an important link between estimated deformations and the possible severity of damage.

Table 1 Relationship between category of damage and limiting tensile strain ε_{lim} (Boscardin and Cording 1989).

Damage category	Normal degree of severity	Limiting tensile strain (mm/m)
0	Negligible (0.1 mm cracks)	0-0.5
1	Very slight (cracks $\leq$ 1 mm)	0.5-0.75
2	Slight (cracks $\leq$ 5 mm)	0.75-1.5
3	Moderate (cracks $\leq$ 15 mm)	1.5-3.0
4 to 5	Severe to very severe (cracks 25 +	>3.0

2.1 Design of the test frame

An imposed load was applied by two Instron hydraulic actuators, of total capacity 100 kN, Figure 1. A spreader beam of height 520 mm was placed between the actuator and the wall, to distribute the load.

For reasons of safety, but also direct comparison with the damage classification in masonry walls, it was decided to simulate in-plane action. Lateral support was provided to limit/prevent lateral displacement, as shown in Figure 1.

The wall setup and dimensions are shown in Figure 2. It was built on a steel H-beam of dimensions $203 \times 203 \times 46$ (in mm), which was used to simulate the founding soils which undergoes settlement, Figure 2(b). The target deflection for the H-Beam was 14 mm in the centre of the 3.11 m span. To realise this deflection, it was decided to pull the simply supported beam down on 2 places 920mm apart. This was done by manually tightening nuts on two rods welded to the H-beam through the specially provided bolt holes in the floor of the laboratory. Care was taken to deform the beam symmetrically, by LVDT measurement during this procedure.

2.2 Measurements

The hydraulic actuators' load cells were used for force monitoring, while LVDT's were applied to measure the foundation beam displacement, as well as the wall lower surface displacement along the wall length, as shown in Figure 3.

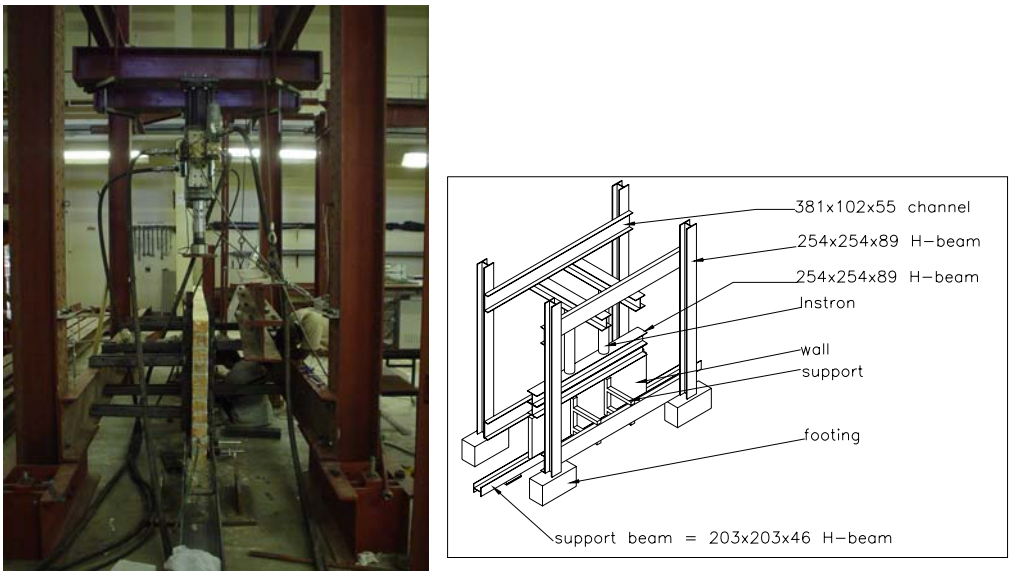

Figure 1 Construction of test apparatus.

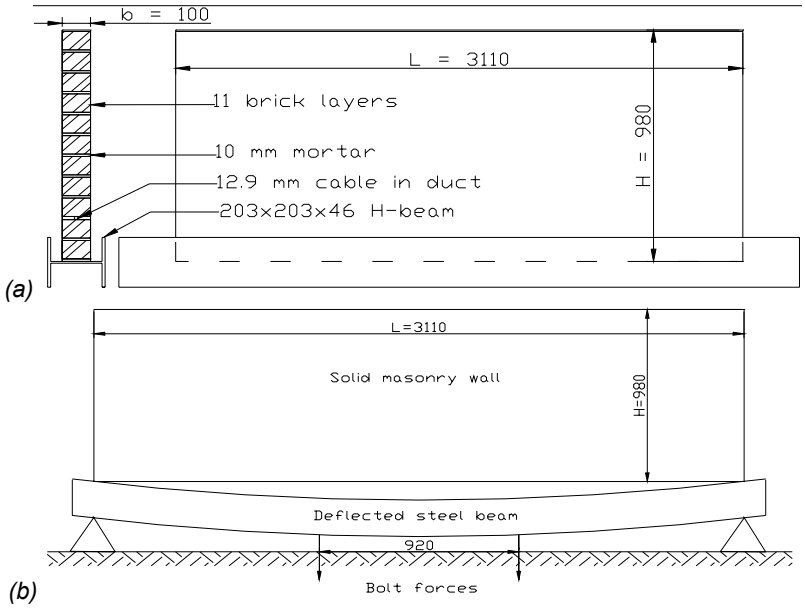

Figure 2 Experimental wall (a) details and (b) Greenfield settlement simulation.

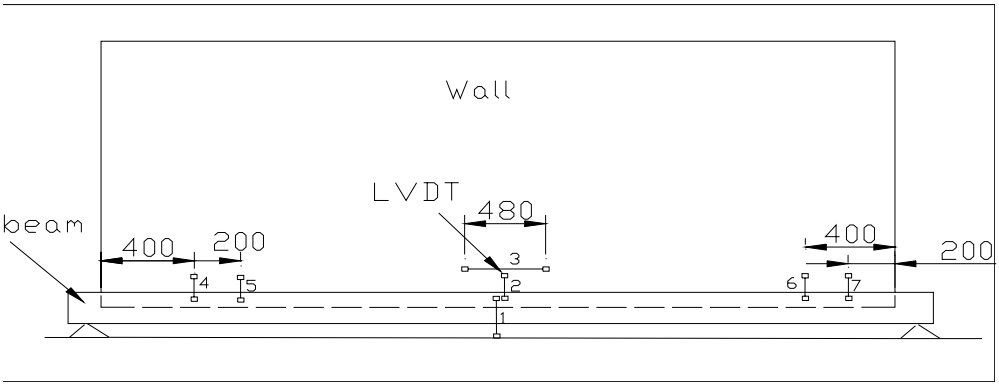

Figure 3 Placement of the 7 LVDT's for wall and foundation displacement monitoring.

2.3 Material property characterisation

The wall was built of solid baked clay bricks and a class II mortar, forming joints of approximately 10 mm thick. To estimate the masonry tensile strength, splitting tests were performed on three bricks, with the results as shown in Table 2.

Table 2 Brick splitting test results and manipulation

Splitting test Mass (kg)		d (mm)	t (mm)	L (mm)	P (kN)	f_{split} (MPa)	f_t (MPa)	$f_{t(lower)}$ (MPa)	$f_{t(upper)}$ (MPa)
1	3.30	71	99	216	47	4.26	2.98	2.32	4.26
2	3.38	73	101	223	35	3.02	2.12	1.65	3.02
3	3.24	72	99	219	48	4.29	3.00	2.34	4.29
					Avg	3.86	2.70	2.10	3.86
					Stdev	0.72	0.51	0.39	0.72
					CoV	18.7%	18.7%	18.7%	18.7%

The splitting test usually overestimates the direct, uniaxial tensile strength f_t, which usually lies in the range $0.06f_{cu} \leq f_t \leq 0.08\ f_{cu}$, say $f_t = 0.07f_{cu}$, while the splitting strength lies in the range $0.08f_{cu} \leq f_{split} \leq 0.11\ f_{cu}$, say $f_{split} = 0.1\ f_{cu}$, where f_{cu} is the compressive strength. By considering these relations, a range for f_t can be calculated to be:
$0.55\ f_{split} \leq f_t \leq 1.0\ f_{split}$ with an average of $f_t = 0.7\ f_{split} = 2.7$ MPa. When the mortar joints are taken into account, the masonry composite tensile strength can be shown to be approximately half the brick strength (Van Zijl et al. 2003).
In the absence of direct measurement, the masonry Young's modulus (**E**) is estimated from the following equation suggested by Hendry et al. (1987):

$$E = cf_c \qquad (1)$$

with c lying in the range $400 \leq c \leq 1500$ and often taken as 700. The masonry composite compressive strength is denoted by f_c. SABS 0164 provides empirical methods to relate the brick strength to the masonry strength. A crushing test was done to determine the value of the brick compressive strength f_{cb} as shown in Table 3.

Table 3 Brick compression test

Compression test nr.	Mass of brick (kg)	L (mm)	t (mm)	Force P (kN)	f_{cb} (MPa)
1	3.24	220	98	830	38.50
2	3.06	216	98	692	32.69
3	3.02	216	99	878	41.06
				average	37.42

From SABS 0164, this masonry crushing strength, together with a class II mortar produces a masonry composite crushing strength of $f_c = 8$ MPa. For c=700, E can then be calculated with eq. (1) as 5600 MPa. For the purpose of this study the Young's modulus was considered to be 3000 MPa. A Poisson's ratio of v = 0.2 was used.

2.4 Experimental procedure

The support beam was deflected by two bolt forces through a distance of 14 mm. Next, the spreader beam of total mass 553 kg, on which the forces by the Instron actuators would be applied, was put onto the wall. Then, the Instrons were used to increase the load on the wall by displacement control. The imposed load was increased incrementally and the wall was inspected for each increment.

3 Experimental results

The gap between the wall and the support beam, as measured by LVDT's 2, 4-7 are shown in Figure 4 for increments of 2.5 kN/m of the applied top load. Notice that the

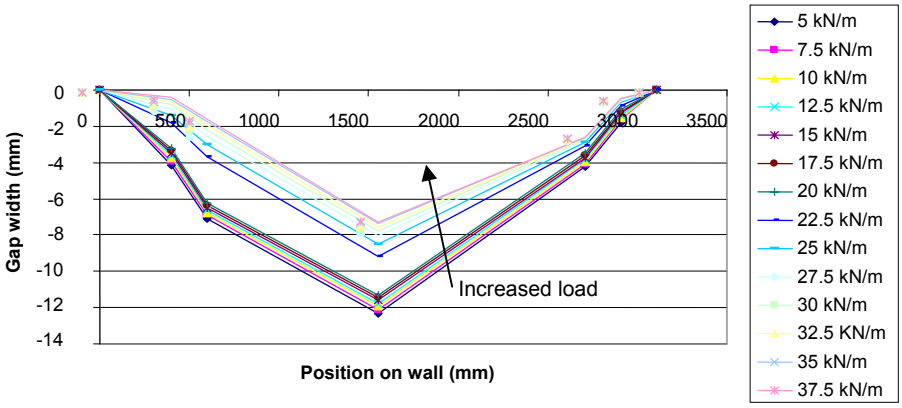

Figure 4 Distance between beam and wall base for increasing load increments.

initial application of the settlement trough led to wall bridging, with a maximum gap between the wall base and the foundation beam of approximately 12 mm. This gap reduced with increased top load, as seen in the figure.

There were no signs of damage up to a load of 22.3 kN/m (own weight plus spreader beam included). At that load the wall cracked 675 mm from its left edge, Figure 5. Due to the asymmetric crack, the gap tended to close left of the crack, as seen in Figure 4.

The maximum deflection (LVDT 1), expressed as a portion of the span length, the so-called deflection ratio, is shown in Figure 6 as function of the total load. The initial low slope in Figure 6 is due to crushing of the mortar layer on which the wall was built and to some extent due to the compression of the plastic casing/duct of a steel cable built into the mortar joint between layers 2 and 3 (Figure 2) for intended repair of the wall in future research.

Imposed load (kN/m)	Crack with (mm)
18.84	0
18.84	2.5
21.66	5.5
24.55	6
35.69	7

Figure 5 Crack observed in wall at position 675 mm from left edge.

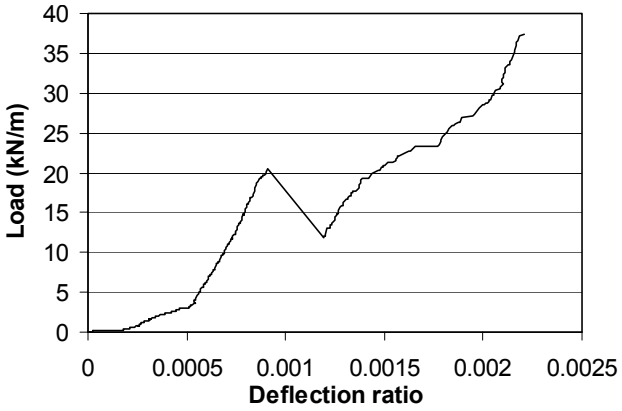

Figure 6 Load - deflection ratio response of the wall.

4 Interpretation of Experiment

In deflection calculations for simple elastic beams with **L/H** ratios larger than 10, only the influence of bending is usually taken into account, as the influence of shear is negligibly small. In this study, a deep beam with **L/H** ratio of 3 is investigated, in which the shear contribution may be significant. This motivates the comparison of elastic strains from simple elastic theory with the strains measured with LVDT 3 in the experiment.

4.1 Elastic response

Firstly, the elastic response observed is compared with analytical results, as well as FE computations. From Timoshenko beam theory the following analytical expression can be derived for the deflection ratio:

$$\Delta = \frac{5qL^4}{384EI}\left(1+\left(\alpha\frac{48I}{5AL^2}\right)\left(\frac{E}{G}\right)\right) \qquad (2)$$

where q is the uniformly distributed load, the geometrical parameters are I the moment of inertia, A the area of a vertical cross-section, α is the shear area factor, equalling 1.2 for a rectangular cross-section. The material parameters are represented by E the elasticity modulus and G the shear modulus.

This equation is shown graphically in Figure 7, along with the experimental response. As discussed in the previous section, the initial load-deformation response seen in Figure 6, is ascribed to crushing of the first mortar layer between the steel foundation beam and the first brick layer. This occurred completely during the first phase of loading, which was the settlement simulation by deformation of the steel foundation beam, while only the wall self weight acted. For this extremely stiff soil, in which the settlement was simulated, the wall ends up to be simply supported, with small contact areas at the supports, leading to local crushing there. Once the crushing led to sufficiently larger bearing areas, elastic response of the wall followed, reflected in the steep, linear ascending branch in Figure 6. For comparison with the analytical results, the initial experimental response is corrected for and the latter, linear response extrapolated, see Figure 7. Close agreement between the corrected experimental response and the analytical response is seen. Also, FE analysis of this wall, along the lines described in section 5, produced near identical results with the analytical ones for the linear part of the response.

The strain evolution in the gauge area of LVDT 3 (Figure 3) provides more data for comparison of the observed and predicted linear response. Cirillo et al. (2004a) showed that, for an aspect ratio (L/H) larger than 2 the normal strain distribution along the section at mid-span is approximately linear, while for smaller aspect ratio's, a nonlinear distribution is found, Figure 8. By assuming such linear strain distribution in

the beam studied in this paper, with L/H=3, the bending strain at the level of LVDT 3 can be expressed by

$$\varepsilon_b = \frac{qL^2c}{8EI} \qquad (3)$$

with q the applied, uniformly distributed load, L the wall length, c the distance from the centre of gravity to the position where the strain is calculated (c=340 mm in the experiment) and I the wall moment of inertia. The strains computed with eq. (3), given the wall geometry and material properties in section 2, are compared in Figure 9 with the strains calculated from the LVDT 3 displacement measurements. Note that a LVDT of relative large range (20mm) was used, leading to a low resolution in the experimental range (0.1mm) of LVDT 3. Nevertheless, the measurements are an indication of the strain evolution. The analytical and experimental strains are in agreement until the wall cracks, after which the experimental strains are arrested, because the crack was outside the gauge area.

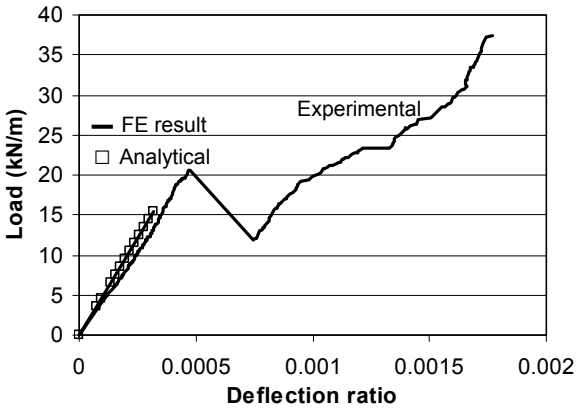

Figure 7 Comparison of the experimental and analytical (eq. 2) displacement ratio's.

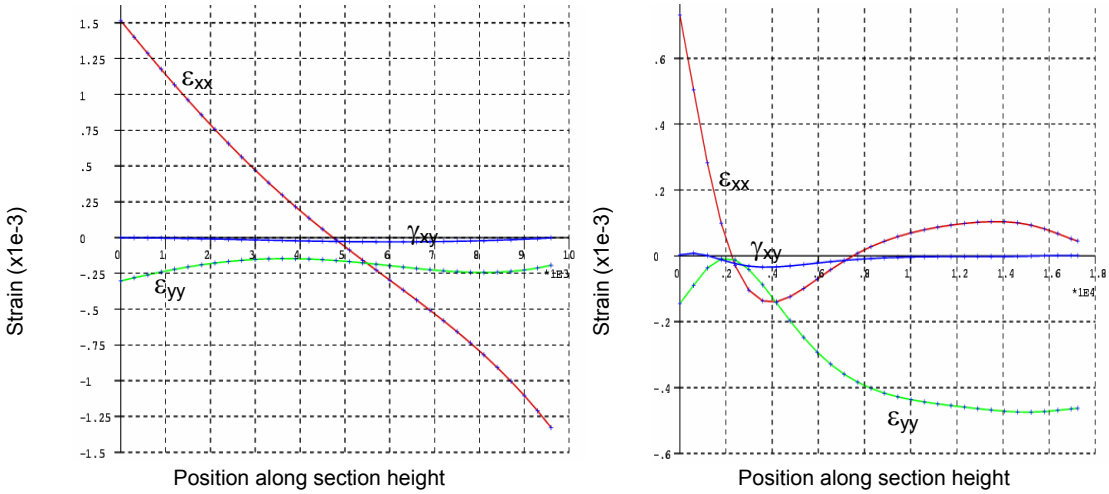

*Figure 8 Normal horizontal ε_{xx} and vertical ε_{yy} , as well as shear γ strains for a deep beam model of (a) **L/H** = 2 and (b) **L/H**=0.5 over its depth at mid-span (Cirillo et al. 2004).*

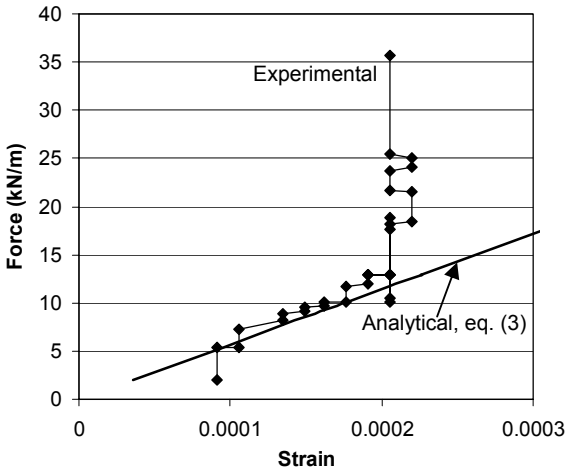

Figure 9 Experimental and analytical (eq. 3) strains at mid-span, low down in the wall.

4.2 Inelastic response

As can be seen in the test, the wall cracked and failed 675 mm from the left edge of the wall and not at mid-span, as might be expected. This phenomenon is ascribed to spatial variation in material properties, combined with deep beam behaviour, for which the normal stress does not increase proportionally to the bending moment from the support to mid-span. Instead, a nearly uniform normal stress distribution along the wall bottom edge is found, as shown by FE analysis results shown in Figure 10.

The superimposed load at which the wall cracked was 18.8 kN/m (total load, including the wall self weight and spreader beam, 22.3 kN/m). From eq. (3) this load coincides with a maximum bending strain of 0.06%. This strain agrees with the range of tensile strain for damage category 1 in Table 1. The crack instantly opened to a width of 2.5 mm, moving it to damage class 2. Upon subsequent load increase, the damage was increased to category 3, according to the crack widths listed in Figure 5.

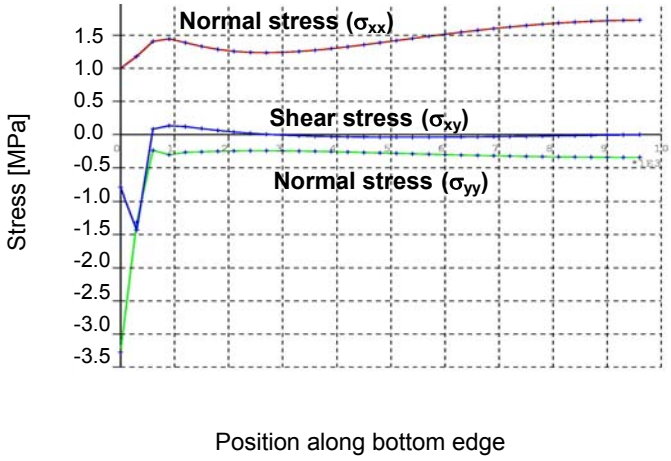

Figure 10 Elastic stress distribution along deep beam (L/H=3) bottom edge from the support (left) to mid-span (right).

5 Nonlinear Finite Element Analysis

The effect of stress re-distribution, crack initiation and propagation was considered by activating a nonlinear material law for the masonry in the finite element analyses. An anisotropic Rankine-Hill model (Lourenço et al. 1998), which captures the different tensile strength parallel to bed joints (f_{tx}) from the low tensile strength perpendicular to be joints (f_{ty}), was used, Figure 11. The horizontal masonry tensile strength f_{tx} was

taken as half of the brick tensile strength derived from the brick splitting tests in section, 2.2, Table 2. No information was available for the bond strength, which limits the vertical tensile resistance. A typical value of 0.25 MPa was employed. For lack of information, equal compressive strength in the two orthogonal directions were prescribed (f_{cx}, f_{cy}), employing the value derived from the brick crushing strengths in section 2.2, Table 3.

The strength reduction after the respective strains corresponding to the peak stresses in both tension and compression, as well as in both material directions, is governed by fracture energies $\mathbf{G_{tx}}$ and $\mathbf{G_{ty}}$ respectively for the two orthogonal directions in tension, and in compression by $\mathbf{G_{cx}}$ and $\mathbf{G_{cy}}$. See Table 4 for the values of these parameters.

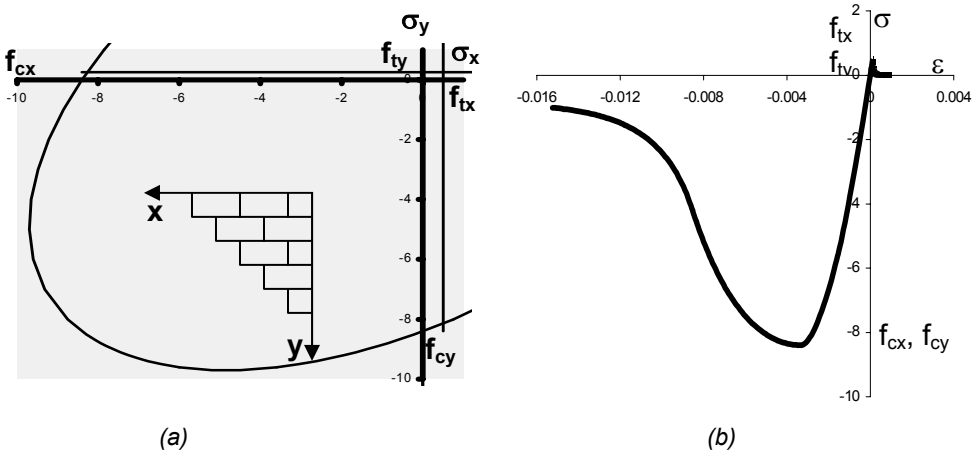

Figure 11 (a) Rankine-Hill strength limit function. (b) Stress-strain laws.

Table 4 Material parameters for the masonry nonlinear behaviour.

f_{tx} (MPa)	f_{ty} (MPa)	f_{cx} (MPa)	f_{cy} (MPa)	G_{tx} (N/mm)	G_{ty} (N/mm)	G_{cx} (N/mm)	G_{cy} (N/mm)
1.0	0.25	8.4	8.4	0.03	0.01	20	20

The numerical (FE) load - deflection ratio response is compared with the experimental response in Figure 7. For simplicity, no attempt was made to simulate the initial low load-deformation slope (Figure 6) associated with crushing of the mortar layer between the foundation beam and the wall.

5.1 Limit load prediction

The analysis predicted crack initiation and instant propagation at a uniform imposed load of 12.0 kN/m (15.4 kN/m, including self weight and spreader beam). The wall in the test was stronger and cracked at 18.8 kN/m (22.3 kN/m). This difference between the computed and measured cracking load is probably caused by the tensile strength being higher than the modelled 1 MPa. This value coincides with the lower limit of the tensile strength estimation in Table 2. If, in stead, the average value derived in Table 2 from the brick splitting strength is accepted, namely f_{tb} = 2.7 MPa, a masonry composite horizontal tensile strength of 1.35 MPa should be used. Linear extrapolation predicts a cracking load of 20.9 kN/m, which is in good agreement with the experimental value. It should be noted that the numerical method predicted the crack to arise at mid-span, where the maximum normal stress occurs, according to Figure 10. No attempt was made to "seed" a crack in the experimentally observed position, by prescribing material of lower strength in that region. Such discrepancy in the crack location is due to the variation in material properties and, in the case of this deep beam, the near uniform normal stress distribution along the wall lower edge, see Figure

10. Nevertheless, the global load-deformational response is predicted with acceptable accuracy.

5.2 Limiting deflection ratio

It can be shown that the maximum bending strain in an elastic deep beam is related to the deflection ratio by

$$\frac{\Delta}{L} = \left(\left(\frac{5}{24} \right) \left(\frac{L}{H} \right) + \left(\frac{1}{5} \right) \left(\frac{H}{L} \right) \left(\frac{E}{G} \right) \right) \varepsilon_{b\max} \qquad (4)$$

The strain at which first cracking will occur is the strain coinciding with the maximum tensile stress, or $\varepsilon_{bmax}=f_{tx}/E$ = 0.45 mm/m. With this strain value substituted into eq. (4) a deflection ratio of 0.00045 is computed. This is in close agreement with the experimental value (0.00047) in Figure 7 at the first crack. Also, if the FE result in Figure 7 is extrapolated for the increased tensile strength of 1.35 MPa, the analytical deflection rate at first cracking is reproduced. Recently, Cirillo et al. (2004) performed nonlinear FE analyses along the lines described in this section, on large walls of dimension L=19.8m, H=6.6m (L/H=3), thickness = 300 mm. Furthermore, the nonlinear parameters were the same as in Table 4, except the tensile strength, which was f_{tx} = 0.5 MPa. The limiting deflection ratio for these large walls were computed as 0.0094% and 0.0096% respectively for founding soil stiffnesses of 10 MN/m^3 and 80 MN/m^3. This independence of the limit deflection ratio on soil stiffness is confirmed by the experiment, which was founded on a “soil” of infinite stiffness. By applying geometrical and material scaling via eq. (4) to the experimental deflection ratio, a value of 0.0103% is predicted. This proves that wall damage is governed by its own relative deflection and not the soil deflection caused by volume loss due to tunnelling.

6 Conclusion

By linear and nonlinear finite element analysis and experimental verification, the shortcomings of simple damage classification models have been highlighted:

1. Masonry walls are brittle, causing instant growth of cracks to large widths, for instance transgressing damage classes 1 to 3 for the 3m long by 1 m high wall investigated. Hereby, the use of a maximum tensile strain derived from the depth of a settlement trough, is not appropriate. Rather, friction and constraint by other buildings or parts of the same structure govern the eventual crack width.
2. The stiffness of the founding soil does not influence the wall deflection ratio which initiates cracking. On the other hand, in softer soil a larger volume loss, or soil deflection is required to cause damage in a wall. This is caused by the wall settling into softer soil, reducing the effective deflection ratio the wall needs to bridge.

References

Burland, JB and Wroth CP (1974). Conference on Settlement of structures, Cambrigde, Pentech Press, London.

Boscardin MD and Cording EJ (1989). Journal of Geotechnical Engineering, Vol. 115, No1, January.

Cirillo, G.P.J., van Zijl, G.P.A.G. and Netzel, H. 2004, Soil-structure interaction in settlement-induced damage to solid masonry walls. This proceedings.

Cirillo, G.P.J., van Zijl, G.P.A.G. and Netzel, H. 2004a, Classification of settlement-induced damage in solid masonry walls: Comparison of FE analysis and analytical strain results. This proceedings.

Hendry, A.W., Sinha, B.P. and Davies, S.R. (1987). *Load Bearing Brickwork Design.* 2nd edition. John Wiley & Sons, New York.

SABS 0164 (1980). South African Standard Code of Practice for The structural use of masonry. Part I: Unreinforced masonry walling.

Van Zijl G.P.A.G., de Vries P.A. and Vermeltfoort A.T. (2003). Masonry wall damage by restraint to shrinkage. *ASCE Journal of Structural Engineering* (in print).